Scientia Iranica A (2016) 23(6), 2458–2468

Sharif University of Technology
Scientia Iranica
Transactions A: Civil Engineering
www.scientiairanica.com

RPIM and RPIM-MLS-based MDLSM method for the solution to elasticity problems

S. Nikravesh[a,*], M.H. Afshar[a] and S. Faraji[b]

a. *School of Civil Engineering, Iran University of Science and Technology, Narmak, Tehran, Iran.*
b. *Department of Civil & Environmental Engineering, Amirkabir University of Technology, 424 Hafez Ave, Tehran, Iran.*

Received 17 November 2014; received in revised form 4 August 2015; accepted 19 October 2015

KEYWORDS
Mesh-free method;
MDLSM method;
Radial Point Interpolation Method (RPIM);
Moving Least-Squares approximation (MLS);
Coupled method.

Abstract. One of the main difficulties in the development of meshless methods using the Moving Least-Squares approximation, such as Mixed Discrete Least-Squares Meshless (MDLSM) method, is the imposition of the essential boundary conditions. In this paper, the RPIM shape function, which satisfies the properties of the Kronecker delta condition, is employed in the Mixed Discrete Least-Squares Meshless (MDLSM) method for solving the elasticity problems. Accordingly, two new MDLSM formulations are proposed in this article, namely RPIM-based MDLSM and coupled MLS-RPIM MDLSM formulation. The essential boundary conditions can be imposed directly on the both presented methods. The proposed methods are used for the solution of three benchmark elasticity problems, and the results are presented and compared with the available analytical solutions and those of MLS-based MDLSM formulations. In addition, in each example, different types of nodal distributions, uniform, and refined configurations are considered to test the performance of the presented methods. The numerical tests indicate higher accuracy of the suggested approaches in comparison with the MLS-based MDLSM method.

1. Introduction

In the past decades, a group of so-called meshless or mesh-free methods has become one of the hottest areas of research in computational mechanics. The main objective of meshless methods is to alleviate the constrained structure of the mesh and to construct the approximation entirely in terms of nodes. Various meshless methods have been introduced and developed to solve different PDE problems that cannot be easily treated by traditional Finite Element Method (FEM).

Some of the well-known meshless methods can be listed here such as Diffuse Element Method (DEM) [1], the Element-Free Galerkin (EFG) method [2], the point interpolation meshless method based on radial basis functions (RPIM) method [3], the Reproducing Kernel Particle Meshless (RKPM) method [4], Moving Particle Semi-implicit (MPS) method [5], and Meshless Local Petrov-Galerkin (MLPG) method [6].

A Discrete Least-Squares Meshless method (DLSM) was proposed by Arzani and Afshar [7] to solve the elliptic problems. Unlike the EFG method which requires background mesh for numerical integration procedure, this method did not involve any integration procedure; therefore, it did not need any background mesh. The method was later extended to simulate free surface problems [8]. The Collocated Discrete Least-Squares Meshless (CDLSM) [9,10] method was later proposed to improve the accuracy of the DLSM method and used to solve elasticity and fluid flow problems. A Mixed Discrete Least-Squares Meshless (MDLSM) method has been recently introduced [11,12] for an effective solution to planer elasticity problems.

*. *Corresponding author.*
E-mail addresses: nikravesh@civileng.iust.ac.ir (S. Nikravesh); mhafshar@iust.ac.ir (M.H. Afshar); saebfaraji@aut.ac.ir (S. Faraji)

Furthermore, a number of robust, adaptive refinement techniques have been recently presented in order to improve the efficiency of the MDLSM method [13-15].

The original DLSM and MDLSM method use the Moving Least-Squares (MLS) approximation to construct shape functions. One of the main difficulties in the implementation of MLS-based meshless approaches, such as MDLSM method, is the imposition of the essential boundary conditions since the MLS shape functions, in general, do not satisfy the Kronecker delta condition. Therefore, the essential boundary conditions cannot be directly enforced in the MDLSM method. For this, the penalty method [11] has been used to impose the essential boundary conditions on MDLSM approach. The penalty coefficient must be chosen large enough in order to impose the boundary conditions, but it should not exceed the maximum value so that it could avoid ill-posed coefficient matrices. This maximum value is different depending on machines precision and numerical method used.

The radial point interpolation shape functions (RPIM) was employed by GR Liu and Gu in meshfree weak-form methods [3,16]. The major advantage of RPIM is that the shape function possesses the Kronecker delta properties paving the way for easier implementation of the essential boundary conditions. Recently, a coupled EFG-RPIM method is proposed to resolve the problem of enforcing the essential boundary conditions in EFG method using RPIM approximation [17].

In this paper, the RPIM shape functions are employed in the MDLSM method to solve the elasticity problems. In order to use RPIM in MDLSM formulation, two different approaches are proposed in this article. In the first approach, the unknown nodal parameters are approximated using the RPIM shape functions; in the second approach, coupled MLS-RPIM shape functions are used in which the RPIM approximation is only applied to the boundary nodes with the MLS shape functions used for the interior nodes. Both formulations allow for direct imposition of the essential boundary conditions removing the need for the penalty method. Performances of the proposed methods are tested by three benchmark examples from the literature on regular and adapted nodal distributions, and the results are presented and compared with those of available analytical solutions. The results indicate the superior accuracy of the proposed methods compared to the conventional MDLSM. Furthermore, it is shown that the RPIM-based formulation is more flexible and accurate than the conventional and coupled MLS-RPIM formulation on the adapted nodal arrangements, while the coupled MLS-RPIM formulation shows a better performance than the RPIM-based formulation on the regular nodal distributions.

The layout of the paper is as follows. In Section 2, the RPIM shape function is introduced. The original MDLSM and proposed formulations using RPIM approximation for solving elasticity problems are given in Section 3. The numerical results are presented in Section 4. And, finally, some concluding remarks are addressed in Section 5.

2. Meshless shape functions

Several techniques have been developed to construct shape functions for meshless methods [16]. In this section, the RPIM shape function, used in the proposed approaches, is presented as follows:

2.1. Radial point interpolation shape functions (RPIM)

The RPIM was employed by GR Liu and Gu in weak-form meshless methods [3,16]. In this method, the unknown function $\boldsymbol{\phi}(\mathbf{X})$ is approximated by:

$$\boldsymbol{\phi}(\mathbf{X}) = \sum_{i=1}^{n} R_i(\mathbf{X})a_i + \sum_{j=1}^{m} P_j(\mathbf{X})b_j = \mathbf{R}^T(\mathbf{X})\mathbf{a} + \mathbf{P}^T(\mathbf{X})\mathbf{b}, \quad (1)$$

with the constraint condition as:

$$\sum_{i=1}^{n} P_j(\mathbf{X}_i)a_i = 0 \quad (j = 1, 2, ..., m), \quad (2)$$

where a_i and b_j are the unknown interpolation constants, m is the number of polynomial basis functions, $P_j(\mathbf{X})$ is monomial in the space coordinate $\mathbf{X} = (x, y)$, n is the number of nodes in the support domain of point $\mathbf{X}$, and $R_i(\mathbf{X})$ is the Radial Basis Function (RBF).

There are many types of radial basis functions. In this paper, Multi-Quadrics Radial Basis Function (MQ-RBF) is employed as follows:

$$R_i(\mathbf{X}) = (r_i^2 + (\beta d_c)^2)^q, \quad (3)$$

where d_c is the characteristic length attributed to the nodal distribution, β and q are the RBF dimensionless shape parameters, and $r_i = \sqrt{(x - x_i)^2 + (y - y_i)^2}$. The shape parameters of MQ-RBF can highly affect the performance of the RPIM approximation. In this paper, value $q = 1.03$ is used, which was suggested by Wang and Liu [18]. Preliminary numerical tests on different examples indicated that the value of $\beta = 3$ leads to better results in the analysis of the 2D elasticity problems by MDLSM method.

Constants a_i and b_j in Eq. (1) are then determined by enforcing Eq. (1) to be satisfied at n nodes in the influence domain of point $\mathbf{X}$. Eqs. (1) and (2) can be re-written in matrix form as:

$$\bar{\boldsymbol{\phi}} = \mathbf{GC} \rightarrow \mathbf{C} = \mathbf{G}^{-1}\bar{\boldsymbol{\phi}}, \quad (4)$$

where:

$$\mathbf{C^T} = \begin{bmatrix} a_1 & a_2 & \dots & a_n & b_1 & b_2 & \dots & b_m \end{bmatrix}_{1\times(n+m)},$$

$$\bar{\boldsymbol{\phi}}^{\mathbf{T}} = \begin{bmatrix} \phi_1 & \phi_2 & \dots & \phi_n & 0 & 0 & \dots & 0 \end{bmatrix}_{1\times(n+m)}.$$

And, the matrix $\mathbf{G}$ in Eq. (4) is defined as follows:

$$\mathbf{G} = \begin{bmatrix} \mathbf{R_0} & \mathbf{P_m} \\ \mathbf{P_m^T} & \mathbf{0} \end{bmatrix}_{(n+m)\times(n+m)}, \tag{5}$$

where $\mathbf{R_0}$ and $\mathbf{P_m}$ are defined as:

$$\mathbf{R_0} = \begin{bmatrix} R_1(r_1) & R_2(r_1) & \cdots & R_n(r_1) \\ R_1(r_2) & R_2(r_2) & \cdots & R_n(r_2) \\ \vdots & \vdots & \ddots & \vdots \\ R_1(r_n) & R_2(r_n) & \cdots & R_n(r_n) \end{bmatrix}_{n\times n}, \tag{6}$$

and:

$$\mathbf{P_m^T} = \begin{bmatrix} 1 & 1 & \cdots & 1 \\ x_1 & x_2 & \cdots & x_n \\ y_1 & y_2 & \cdots & y_n \\ \vdots & \vdots & \ddots & \vdots \\ P_m(\mathbf{x}_1) & P_m(\mathbf{x}_2) & \cdots & P_m(\mathbf{x}_n) \end{bmatrix}_{m\times n} \tag{7}$$

Since the matrix $\mathbf{R_0}$ is symmetric, the matrix $\mathbf{G}$ will also be symmetric. Eq. (1) can be re-written using Eq. (4) as follows:

$$\boldsymbol{\phi}(\mathbf{X}) = \mathbf{R}^T(\mathbf{X})\mathbf{a} + \mathbf{P}^T(\mathbf{X})\mathbf{b} = \begin{bmatrix} \mathbf{R}^T(\mathbf{X}) & \mathbf{P}^T(\mathbf{X}) \end{bmatrix} \mathbf{C}$$

$$\rightarrow \boldsymbol{\phi}(\mathbf{X}) = \begin{bmatrix} \mathbf{R}^T(\mathbf{X}) & \mathbf{P}^T(\mathbf{X}) \end{bmatrix} \mathbf{G^{-1}}\bar{\boldsymbol{\phi}}, \tag{8}$$

where the RPIM shape functions can be shown as:

$$\begin{aligned} \bar{\mathbf{N}}^T(\mathbf{X}) &= \begin{bmatrix} \mathbf{R}^T(\mathbf{X}) & \mathbf{P}^T(\mathbf{X}) \end{bmatrix} \mathbf{G^{-1}} \\ &= [N_1(\mathbf{x})\ N_2(\mathbf{x})\ \cdots\ N_n(\mathbf{x})\ N_{n+1}(\mathbf{x}) \\ &\quad \cdots\ N_{n+m}(\mathbf{x})]. \end{aligned} \tag{9}$$

Hence, the RPIM shape functions corresponding to the n unknown nodal values are obtained as:

$$\mathbf{N}^T(\mathbf{X}) = \begin{bmatrix} N_1(\mathbf{x}) & N_2(\mathbf{x}) & \cdots & N_n(\mathbf{x}) \end{bmatrix}. \tag{10}$$

The RPIM shape functions can be calculated in an alternative form by solving Eq. (4) and substituting the solution into Eq. (1):

$$\begin{aligned} \mathbf{N}^T(\mathbf{X}) &= \mathbf{R}^T(\mathbf{X})\mathbf{G}_a + \mathbf{P}^T(\mathbf{X})\mathbf{G}_b \\ &= \begin{bmatrix} N_1(\mathbf{x}) & N_2(\mathbf{x}) & \cdots & N_n(\mathbf{x}) \end{bmatrix}. \end{aligned} \tag{11}$$

where:

$$\mathbf{G}_b = (\mathbf{P_m}^T\mathbf{R_0}^{-1}\mathbf{P_m})^{-1}\mathbf{P_m}^T\mathbf{R_0}^{-1}, \tag{12}$$

and:

$$\mathbf{G}_a = \mathbf{R_0}^{-1}(\mathbf{I}_{n\times n} - \mathbf{P_m}\mathbf{G_b}). \tag{13}$$

The RPIM shape functions pass through the nodal values. Therefore, RPIM shape functions, given in Eq. (10), possess the Kronecker delta property.

More detailed information on the RPIM approximation and the Radial Basis Functions (RBF) can be found elsewhere [3,16,18,19].

3. Mixed discrete least-squares meshless method for elasticity

The conventional MDLSM and proposed formulations using RPIM approximation for solving elasticity problems are given in this section.

3.1. MLS-based MDLSM formulation

Consider the following partial differential equation governing 2D linear elasticity problems [20]:

$$-\mu\Delta\mathbf{u} - (\mu+\lambda)\nabla(\nabla.\mathbf{u}) = \mathbf{f} \quad \text{in } \Omega, \tag{14}$$

with the following displacement and traction boundary conditions:

$$\begin{cases} u = u^* \\ \qquad\qquad \text{on } \Gamma_u \\ v = v^* \end{cases}$$

$$\begin{cases} \sigma_x n_x + \tau_{xy} n_y = t_x^* \\ \qquad\qquad\qquad\qquad \text{on } \Gamma_t \\ \tau_{xy} n_x + \sigma_y n_y = t_y^* \end{cases} \tag{15}$$

where Ω is the problem domain that incorporates an elastic material; Γ_t and Γ_u are the traction and displacement boundaries, respectively; n_x and n_y are direction cosines of the normal to the boundary; t_x^*, t_y^* and u^*, v^* are components of the prescribed tractions and displacements in the Cartesian coordinate system, respectively.

The parameters λ and μ are the Lame constants defined for plain stress problems as:

$$\lambda = \frac{Ev}{(1-2v)(1+v)} > 0 \quad \text{and} \quad \mu = \frac{E}{2(1+v)} > 0, \tag{16}$$

where E is the elasticity modulus and v is the Poisson ratio.

In addition, stresses can be defined in terms of the displacement components as follows:

$$\sigma_x = (\lambda+2\mu)\frac{\partial u}{\partial x} + \lambda\frac{\partial v}{\partial y},$$

$$\sigma_y = \lambda\frac{\partial u}{\partial x} + (\lambda+2\mu)\frac{\partial v}{\partial y},$$

$$\tau_{xy} = \mu\left(\frac{\partial u}{\partial y} + \frac{\partial v}{\partial x}\right). \tag{17}$$

Rewriting Eq. (14) in terms of stresses leads to:

$$\frac{\partial \sigma_x}{\partial x} + \frac{\partial \tau_{xy}}{\partial y} = -f_x \quad \text{in } \Omega,$$

$$\frac{\partial \tau_{xy}}{\partial x} + \frac{\partial \sigma_y}{\partial y} = -f_y \quad \text{in } \Omega. \tag{18}$$

Eqs. (17) and (18) can be rewritten in a matrix form as follows:

$$\mathbf{S}(\boldsymbol{\phi}) + \mathbf{F} = 0, \tag{19}$$

where $\boldsymbol{\phi}$ and $\mathbf{F}$ are vectors of unknowns and forcing terms defined as:

$$\boldsymbol{\phi} = \begin{bmatrix} u & v & \sigma_x & \sigma_y & \tau_{xy} \end{bmatrix}^T, \tag{20}$$

$$\mathbf{F} = \begin{bmatrix} 0 & 0 & 0 & -f_x & -f_y \end{bmatrix}^T. \tag{21}$$

And, $\mathbf{S}(.)$ is the first-order differential operator defined as:

$$\mathbf{S}(.) = \mathbf{S}_1(.)_x + \mathbf{S}_2(.)_y + \mathbf{S}_3(.), \tag{22}$$

where $\mathbf{S}_1$, $\mathbf{S}_2$, and $\mathbf{S}_3$ are defined by the following matrices:

$$\mathbf{S}_1 = \begin{bmatrix} (\lambda+2\mu) & 0 & 0 & 0 & 0 \\ \lambda & 0 & 0 & 0 & 0 \\ 0 & \mu & 0 & 0 & 0 \\ 0 & 0 & 1 & 0 & 0 \\ 0 & 0 & 0 & 0 & 1 \end{bmatrix},$$

$$\mathbf{S}_2 = \begin{bmatrix} 0 & \lambda & 0 & 0 & 0 \\ 0 & (\lambda+2\mu) & 0 & 0 & 0 \\ \mu & 0 & 0 & 0 & 0 \\ 0 & 0 & 0 & 0 & 1 \\ 0 & 0 & 0 & 1 & 0 \end{bmatrix},$$

$$\mathbf{S}_3 = \begin{bmatrix} 0 & 0 & -1 & 0 & 0 \\ 0 & 0 & 0 & -1 & 0 \\ 0 & 0 & 0 & 0 & -1 \\ 0 & 0 & 0 & 0 & 0 \\ 0 & 0 & 0 & 0 & 0 \end{bmatrix}. \tag{23}$$

The boundary conditions of Eq. (15) are also re-written in a matrix form as:

$$\mathbf{D}\boldsymbol{\phi} - \mathbf{F}^* = 0, \tag{24}$$

where F^* and D are defined as:

$$\mathbf{F}^* = \begin{bmatrix} u^* & v^* & t_x^* & t_y^* \end{bmatrix}, \tag{25}$$

and:

$$\mathbf{D} = \begin{bmatrix} 1 & 0 & 0 & 0 & 0 \\ 0 & 1 & 0 & 0 & 0 \\ 0 & 0 & n_x & 0 & n_y \\ 0 & 0 & 0 & n_y & n_x \end{bmatrix}. \tag{26}$$

The residuals at the typical node i can be defined as:

$$\mathbf{R}_{\Omega_i} = (\mathbf{S}\boldsymbol{\phi})_i + \mathbf{F}_i \quad \text{in } \Omega, \tag{27}$$

$$\mathbf{R}_{\Gamma_i} = (\mathbf{D}\boldsymbol{\phi})_i - \mathbf{F}_i \quad \text{on } \Gamma. \tag{28}$$

A least-squares functional for typical node i can, therefore, be defined using penalty approach:

$$I_i = (\mathbf{R}_\Omega^T \mathbf{R}_\Omega)_i + \alpha (\mathbf{R}_\Gamma^T \mathbf{R}_\Gamma)_i. \tag{29}$$

And, the least-squares functional for the whole domain can be defined as:

$$I^M = \sum_{i=1}^{n_\Omega} (\mathbf{R}_\Omega^T \mathbf{R}_\Omega)_i + \alpha \sum_{i=1}^{n_\Gamma} (\mathbf{R}_\Gamma^T 5 \mathbf{R}_\Gamma)_i, \tag{30}$$

where α condition is the penalty coefficient that should be large enough to satisfy the boundary desired accuracy. n_Ω and n_Γ are the number of nodes in the domain and on the boundaries, respectively.

Minimizing the least-squares functional with respect to the vector of unknown nodal parameters $\boldsymbol{\phi}$ leads to:

$$\mathbf{K}\boldsymbol{\phi} = \mathbf{F}, \tag{31}$$

where:

$$\mathbf{K}_{lm} = \sum_{i=1}^{n_\Omega} \left[\mathbf{S}(\mathbf{N}_l)\right]_i^T \left[\mathbf{S}(\mathbf{N}_m)\right]_i + \alpha \sum_{i=1}^{n_\Gamma} \left[\mathbf{D}(\mathbf{N}_l)\right]_i^T \left[\mathbf{D}(\mathbf{N}_m)\right]_i, \tag{32}$$

and:

$$\mathbf{F}_l = \sum_{i=1}^{n_\Omega} \left[\mathbf{S}(\mathbf{N}_l)\right]_i^T \mathbf{F}_i + \alpha \sum_{i=1}^{n_\Gamma} \left[\mathbf{D}(\mathbf{N}_l)\right]_i^T \mathbf{F}_i^*, \tag{33}$$

where $\mathbf{N}_l$ is the MLS shape function [11] of node l. It can be noted that the MLS approximation generally does not pass through the nodal values. Thus, the MLS shape functions do not satisfy Kronecker delta condition.

More detailed explanations of this shape function can be found elsewhere [11,16].

3.2. Proposed RPIM-based MDLSM formulation

In this approach, the unknown parameters are approximated using the RPIM shape functions. Since RPIM satisfies Kronecker delta property, the displacement boundary conditions can be imposed as conveniently as in conventional FEM, and there is no need for using the penalty method. The stress boundary conditions are enforced via the least-squares functional as follows.

The least-squares functional for the whole domain is defined as:

$$I^R = \sum_{i=1}^{n_\Omega} (\mathbf{R}_\Omega^T \mathbf{R}_\Omega)_i + \sum_{i=1}^{n_\Gamma} (\mathbf{R}_\Gamma^T \mathbf{R}_\Gamma)_i, \tag{34}$$

where the residuals $\mathbf{R}_\Omega$ and $\mathbf{R}_\Gamma$ are defined in Eqs. (27) and (28). Minimizing the least-squares functional with respect to the vector of unknown nodal parameters $\boldsymbol{\phi}$ leads to:

$$\mathbf{K}\boldsymbol{\phi} = \mathbf{F}, \tag{35}$$

where:

$$\mathbf{K}_{lm} = \sum_{i=1}^{n_\Omega} \left[\mathbf{S}(\tilde{\mathbf{N}}_l)\right]_i^T \left[\mathbf{S}(\tilde{\mathbf{N}}_m)\right]_i + \sum_{i=1}^{n_\Gamma} \left[\mathbf{D}(\tilde{\mathbf{N}}_l)\right]_i^T \left[\mathbf{D}(\tilde{\mathbf{N}}_m)\right]_i, \tag{36}$$

and:

$$\mathbf{F}_l = \sum_{i=1}^{n_\Omega} \left[\mathbf{S}(\tilde{\mathbf{N}}_l)\right]_i^T \mathbf{F}_i + \sum_{i=1}^{n_\Gamma} \left[\mathbf{D}(\tilde{\mathbf{N}}_l)\right]_i^T \mathbf{F}_i^*, \tag{37}$$

where $\tilde{\mathbf{N}}_l$ is the RPIM shape function of node l. The final stiffness matrix $\mathbf{K}$ is square $(5N \times 5N)$, symmetric and positive-definite matrix in which N is the total number of nodes.

3.3. Proposed MDLSM formulation using coupled MLS-RPIM shape functions

Consider an arbitrary support domain containing n typical nodes. As shown in section two, MLS approximation requires the solution of $m \times m$ linear equation system, while $n \times n$ linear system should be solved in the RPIM method, where m is the monomial basis functions. Generally, n is much bigger than m; therefore, the computing effort of RPIM is, in general, more than MLS.

In this section, an alternative approach is proposed in order to avoid increased computational cost of solving large-scale problems while improving the efficiency of the boundary condition imposition on MDLSM method. In this approach, coupled MLS-RPIM shape functions are used to approximate the trail functions in which the MLS shape functions are used for the nodes inside the problem domain, and the RPIM approximation is only applied to the boundary nodes. Therefore, The displacement boundary conditions are imposed directly, and the stress boundary conditions are applied via the least-squares functional. This requires the following modifications in the conventional formulation.

In the proposed approach, the least-squares functional is formed as Eq. (34) leading to the matrices $\mathbf{K}_{lm}$ and $\mathbf{F}_l$ defined by Eqs. (35)-(37), with the shape function $\tilde{\mathbf{N}}$ defined by the following condition:

$$\text{If } i \in \{n_\Gamma\} \rightarrow \tilde{\mathbf{N}} = \mathbf{N}^{\text{RPIM}}$$

$$\text{Else} \rightarrow \tilde{\mathbf{N}} = \mathbf{N}^{\text{MLS}}, \tag{38}$$

where $\mathbf{N}^{\text{RPIM}}$ and $\mathbf{N}^{\text{MLS}}$ are the RPIM and MLS shape functions, respectively.

The final stiffness matrix $\mathbf{K}$ is square $(5N \times 5N)$, symmetric and positive definite matrix in which N is the total number of nodes.

4. Numerical examples

In this section, three benchmark examples from elasticity with analytical solution are solved using the proposed RPIM-based MDLSM, MDLSM using coupled MLS-RPIM shape functions, and the original MLS-based MDLSM approaches on uniform and adapted nodal distributions. The results are presented and compared with the available exact solutions. It should be noted that all the adapted configurations are made manually by the engineering judgments. The examples include:

1. Cantilever beam;
2. Cylinder subjected to internal pressure;
3. Infinitive plate with a circular hole.

In this paper, a normalized value of least-squares functional is used as the residual error estimator in which the total residual error e_g is defined as:

$$e_g = \frac{\sqrt{I}}{\sqrt{\boldsymbol{\phi}^T \boldsymbol{\phi}}}, \tag{39}$$

where I is the value of least-square functional defined in Eqs. (30) and (34) for each proposed method, and $\boldsymbol{\phi}$ is the vector of unknowns.

Furthermore, in all problems, the second order polynomial basis $(P = 2, m = 6)$ is used to construct MLS shape functions. The radius of the support domain of node i is calculated as follows:

$$d_w = \rho d_m, \tag{40}$$

where d_m is the distance of mth nearest node to point i, m is the number of terms used in polynomial basis P ($m = 3$ for linear polynomial basis and $m = 6$ for quadratic polynomial basis), and ρ is a constant coefficient that varies between 2 to 3 determined by a trail-and-error procedure. Penalty coefficient used in MLS-based MDLSM method is taken to be $\alpha = 10^8$.

All the problems are solved on an Intel(R) Core(TM)2 Duo T9550 Machine with 2.67GH$_z$ CPU and 6.00 GB of DDR2 RAM.

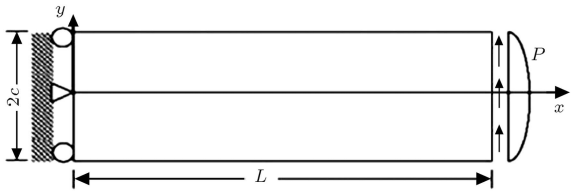

Figure 1. A cantilever beam subjected to load at the end.

4.1. Example 1: Cantilever beam

A cantilever beam subjected to a concentrated load at the free end (Figure 1) is considered as the first example. The analytical solution of this example is available [20] as follows:

$$u = -\frac{Py}{6EJ}\left[3x(2L-x)+(2+v)(y^2-c^2)\right],$$

$$V = \frac{P}{6EJ}\left[x^2(3L-x)+3vy^2(L-x)+(4+5v)c^2x\right]$$

$$\sigma_{xx} = -P\frac{(L-x)y}{J},$$

$$\sigma_{yy} = 0,$$

$$\tau_{xy} = \frac{P}{2J}\left[c^2-y^2\right], \tag{41}$$

where L is the length of the beam, v is the Poisson's ratio, and J is the moment of inertia of the rectangular cross-sectional beam with the unit thickness defined as $J = 2c^3/3$. This example is solved using the proposed approaches and original MDLSM method under the plane stress condition with the following constraints: $P = 1$, $E = 1000$, $v = 0.25$, $L = 8$, and $c = 1$.

In this example, two uniform nodal distributions of 85 and 451 nodes and an adapted configuration containing 364 nodes are considered for solving this problem, as shown in Figure 2. The results are presented and compared in Table 1. In addition, the variation of stress σ_{xx} along the upper boundary and the horizontal displacement u_x along the bottom boundary are plotted for each nodal distribution (Figures 3 and 4). As seen from the results, the MDLSM method using coupled shape functions produces more accurate results on uniform configurations, while the RPIM-based MDLSM has been able to produce more accurate results on the adapted distributions.

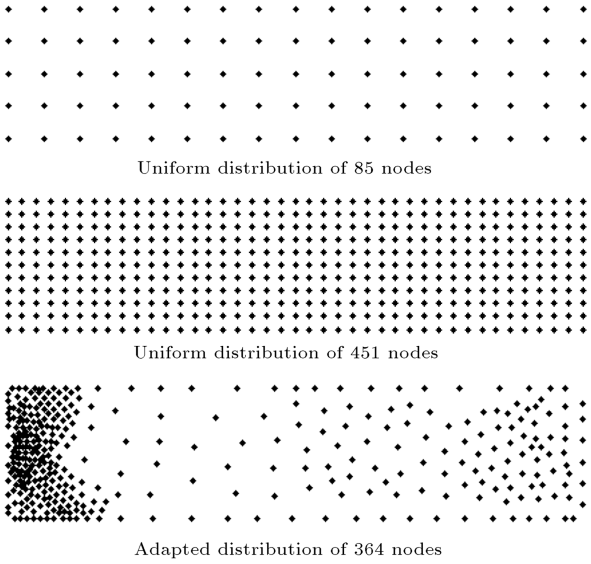

Figure 2. Three nodal configurations (Example 1).

4.2. Example 2: Cylinder subjected to internal pressure

The second example considered in this paper is a cylinder subjected to internal pressure (Figure 5). Due to the symmetry, just a quarter of the cylinder is simulated. The analytical solution of this problem [20] is:

$$\sigma_r = \frac{r_1^2P}{r_2^2-r_1^2}\left(1-\frac{r_2^2}{r^2}\right), \tag{42}$$

$$\sigma_\theta = \frac{r_1^2P}{r_2^2-r_1^2}\left(1+\frac{r_2^2}{r^2}\right). \tag{43}$$

The boundary conditions are shown in Figure 6. This example is solved using the proposed methods with $r_1 = 1$, $r_2 = 5$, $P = 1$, $v = 0.3$, and $E = 1$ under the plane stress condition.

Once again, two uniform nodal distributions of 106 and 765 nodes and an adapted configuration containing 481 nodes are considered for solving this problem, as shown in Figure 7. The results are presented and compared in Table 2. Furthermore, the variation of stress σ_{xx} along $x = 0$ and $y = 0$ boundaries is plotted for each nodal arrangements (Figures 8 and 9). The results illustrate the accuracy of using RPIM shape functions in the MDLSM method.

Table 1. Comparison of total residual errors in Example 1.

Nodal distribution		Total residual error		
		Uniform	Uniform	Adapted
Total number of nodes		85	451	364
Shape functions	MLS	0.0158	0.0050	0.0028
	RPIM	0.0161	0.0040	8.07×10^{-4}
	Coupled MLS-RPIM	0.0068	0.0018	0.0016

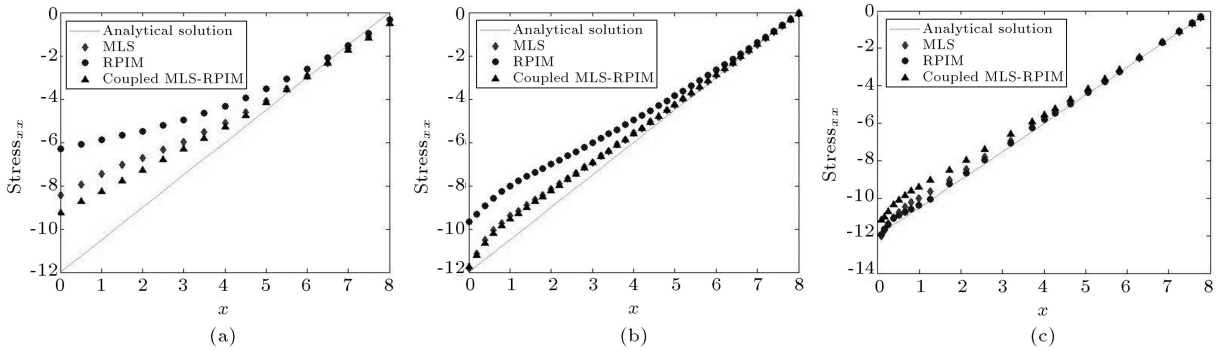

Figure 3. Normal stress σ_{xx} along $y = 1$ (Example 1): (a) Coarse uniform distribution with 85 nodes; (b) fine uniform distribution with 451 nodes; and (c) refined distribution with 364 nodes.

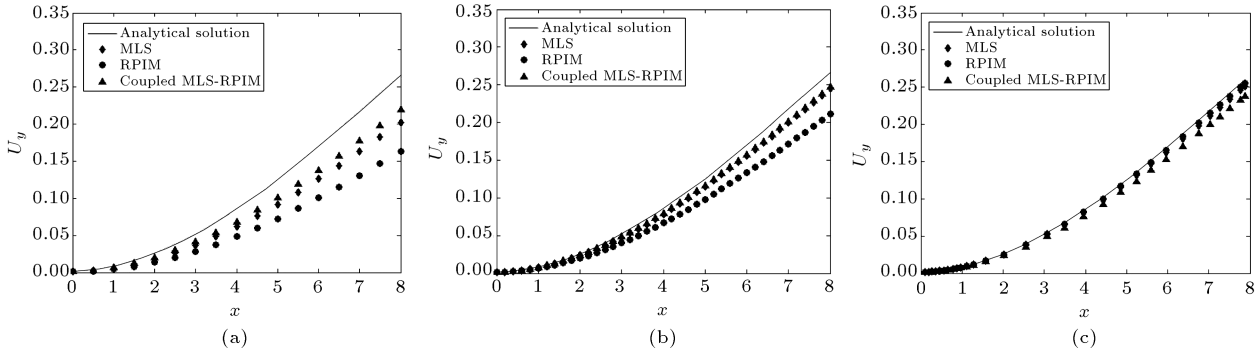

Figure 4. Vertical displacement v along $y = -1$ (Example 1): (a) Uniform distribution with 85 nodes; (b) uniform distribution with 451 nodes; and (c) adapted distribution with 364 nodes.

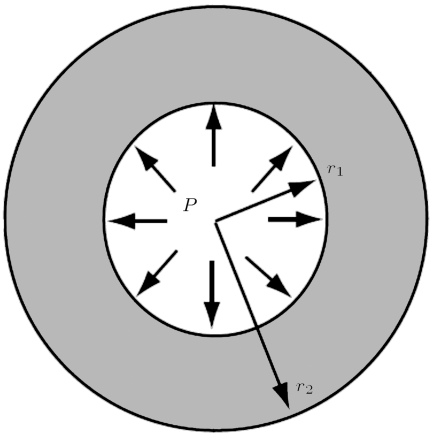

Figure 5. A cylinder subjected to internal pressure.

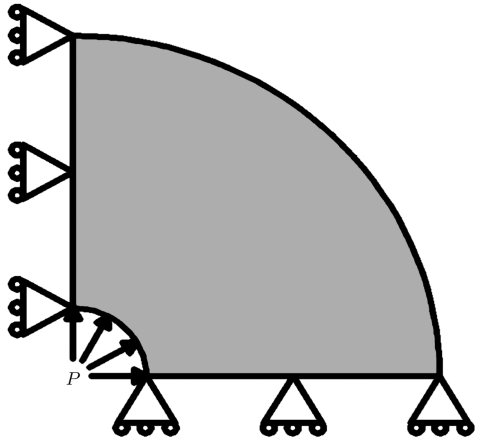

Figure 6. A quarter of the cylinder and its boundary.

Table 2. Comparison of total residual errors in Example 2.

Nodal distribution		Total residual error		
		Uniform	Uniform	Adapted
Total number of nodes		**106**	**765**	**481**
Shape functions	**MLS**	0.1931	0.0095	0.0011
	RPIM	0.2003	0.0109	4.32×10^{-4}
	Coupled MLS-RPIM	0.1099	0.0074	0.0010

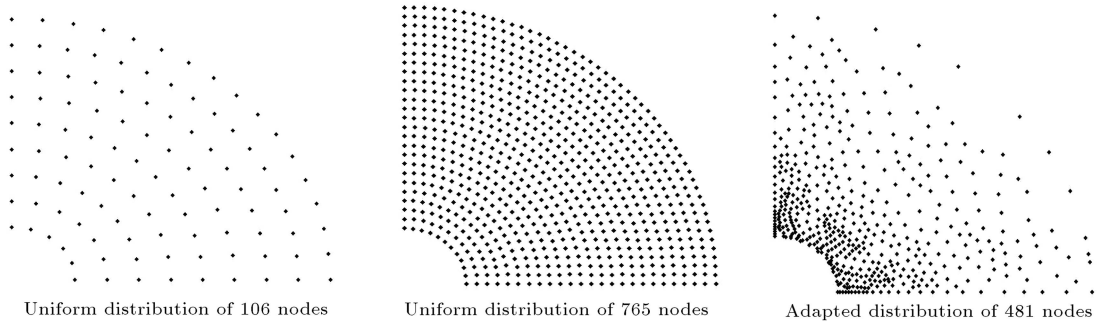

Figure 7. Three nodal configurations (Example 2).

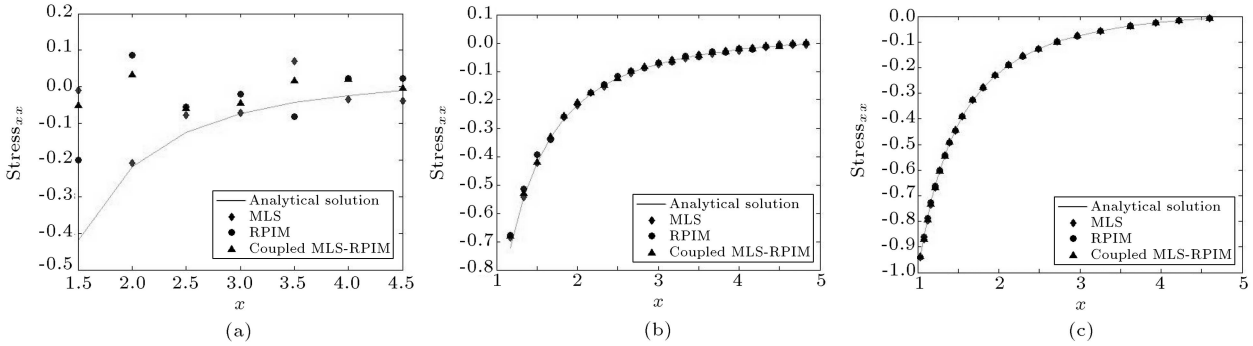

Figure 8. Normal stress σ_{xx} along $y = 0$ (Example 1): (a) Uniform distribution with 106 nodes; (b) uniform distribution with 765 nodes; and (c) adapted distribution with 481 nodes.

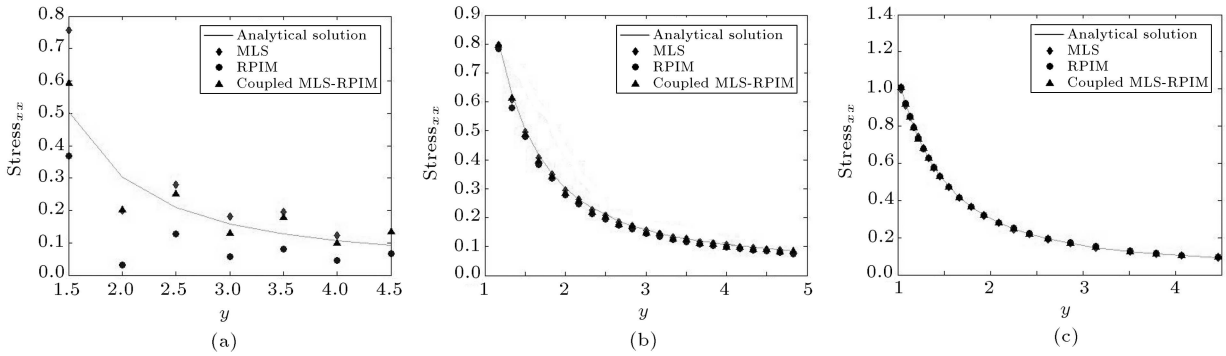

Figure 9. Normal stress σ_{xx} along $x = 0$ (Example 1): (a) Coarse uniform distribution with 106 node; (b) fine uniform distribution with 765 nodes; and (c) refined distribution with 481 nodes.

4.3. Example 3: Infinite plate with a circular hole

The final example considered in this paper is an infinitive plate with a circular hole subjected to a uniaxial traction (t), as shown in Figure 10. The analytical solution for this example is available [20] as follows:

$$u_r = \frac{t}{4G}\left[r\left(\frac{\omega-1}{2}+\cos(2\theta)\right) + \frac{\bar{r}^2}{r}\left(1+55(1+\omega)\cos(2\theta)\right) - \frac{\bar{r}^4}{r^3}\cos(2\theta)\right],$$

$$u_\theta = \frac{t}{4G}\left[(1-\omega)\frac{\bar{r}^2}{r} - r - \frac{\bar{r}^4}{r^3}\right]\sin(2\theta),$$

$$\sigma_{xx} = t\left[1-\frac{\bar{r}^2}{r^2}\left(\frac{3}{2}\cos(2\theta)+\cos(4\theta)\right)+\frac{3\bar{r}^4}{2r^4}\cos(4\theta)\right],$$

$$\sigma_{yy} = -\left[\frac{\bar{r}^2}{r^2}\left(\frac{1}{2}\cos(2\theta)-\cos(4\theta)\right)+\frac{3\bar{r}^4}{2r^4}\cos(4\theta)\right],$$

$$\tau_{xy} = -t\left[\frac{\bar{r}^2}{r^2}\left(\frac{1}{2}\sin(2\theta)+\sin(4\theta)\right)-\frac{3\bar{r}^4}{2r^4}\sin(4\theta)\right], \quad (44)$$

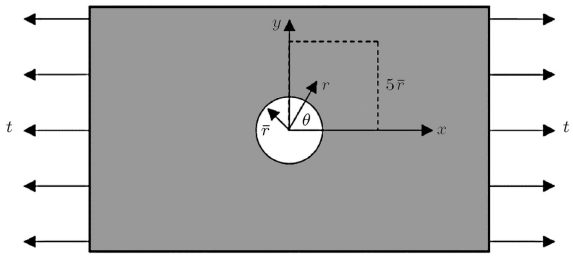

Figure 10. An infinite plate with a circular hole under a uniaxial load t.

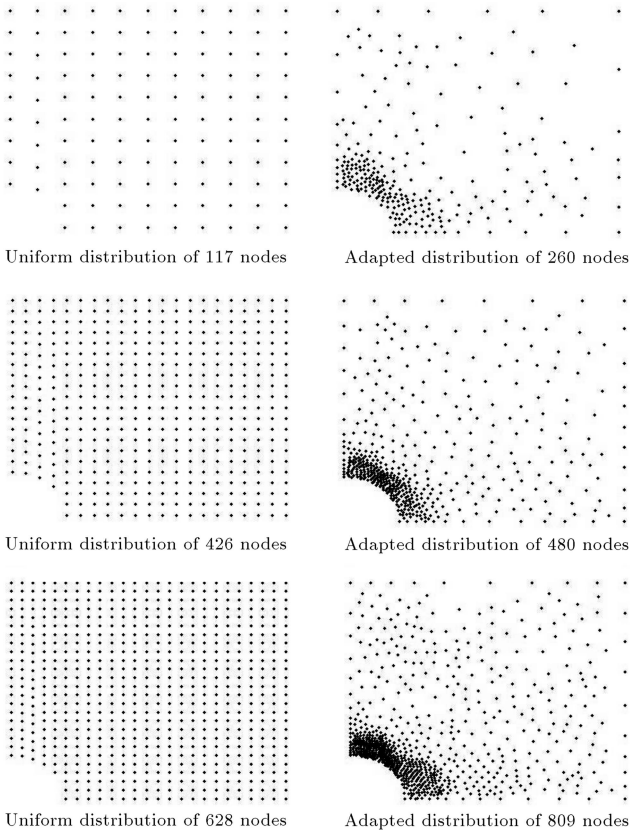

Figure 11. Uniform and adapted nodal configurations (Example 3).

where G is the shear modulus, $\omega = (3 - v)/(1 + v)$, and v is the Poisson's ratio.Due to the symmetry, the problem is solved using only a quarter of the plate with the dimension of $5\bar{r}$ where $\bar{r}$ is the radius of the hole. The symmetry boundary conditions are imposed on the bottom and left boundaries; no traction boundary condition is applied at the hole boundary, and the traction boundary conditions are imposed on the top and right boundaries. This example is solved using $t = 1$, $E = 1000$, and $v = 0.3$ under the plane stress condition.

This example is solved considering three uniform distributions of 117, 426, and 628 nodes and another three adapted distributions of 260, 480, and 809 nodes (Figure 11). The normal stress, σ_{xx}, along $x = 0$ boundary is shown for each nodal arrangement (Figure 12). The residual errors are also compared in Tables 3 and 4. As can be seen from the results, the coupled MLS-RPIM based MDLSM has produced more accurate results on the uniform nodal distributions, while the RPIM-based-MDLSM shows superior performance on the refined configurations.

5. Conclusion

In this paper, the RPIM shape functions are used in the MDLSM method to solve elasticity problems. Two different approaches are suggested to incorporate RPIM in MDLSM formulation, namely the RPIM-based MDLSM and the coupled MLS-RPIM-based MDLSM formulation. In both approaches, the essential boundary conditions can be imposed directly removing the need for penalty methods. The proposed methods were used for the solution of three benchmark elasticity problems, and the results are presented and compared with the available analytical solutions and those of MLS-based MDLSM formulation. Uniform and adapted configurations of different scales are also considered to test the efficiency and reliability of the presented methods. The results indicated that both suggested approaches are, in general, more accurate than the MLS-based formulation. Furthermore, the coupled MLS-RPIM-based MDLSM has indicated more accuracy on the uniform nodal distributions, while the RPIM-based MDLSM has shown more accuracy on the refined configurations.

Table 3. Comparison of total residual error for adapted nodal configurations in Example 3.

Adapted nodal distributions		Total residual error		
		Coarse	Mild	Fine
Total number of nodes		**260**	**480**	**809**
Shape functions	**MLS**	0.0049	0.0016	5.93×10^{-4}
	RPIM	0.0010	2.67×10^{-4}	1.26×10^{-4}
	Coupled MLS-RPIM	0.0046	0.0014	5.57×10^{-4}

Table 4. Comparison of total residual error for uniform nodal configurations in Example 3.

Uniform nodal distributions		Total residual error		
		Coarse	Mild	Fine
Total number of nodes		**117**	**426**	**628**
Shape functions	**MLS**	0.1654	0.0174	0.0128
	RPIM	0.0843	0.0160	0.0096
	Coupled MLS-RPIM	0.0963	0.0144	0.0095

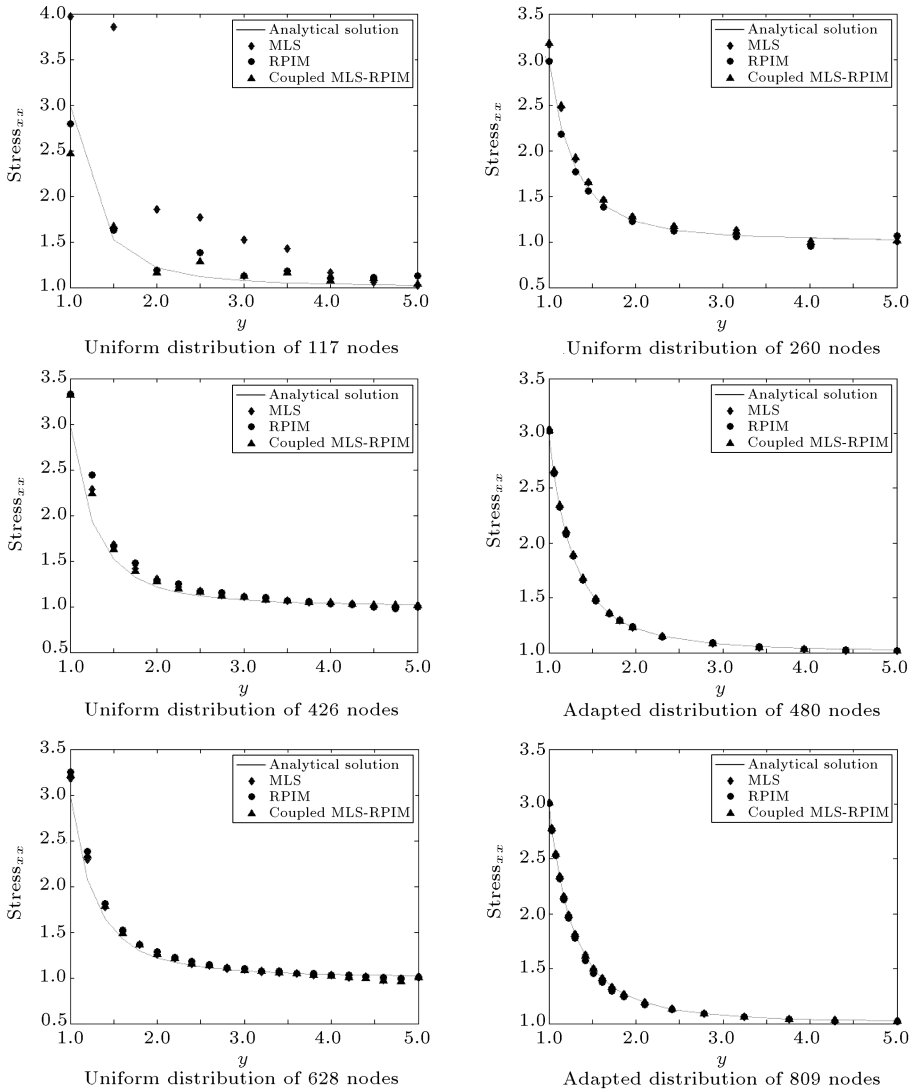

Figure 12. Normal stress σ_{xx} along $x = 0$ (Example 3).

References

1. Nayroles, B., Touzot, G. and Villon, P. "The diffuse elements method", *Comptes Rendus De L Academie Des Sciences Serie Ii*, **313**(2) pp. 133-138 (1991).
2. Belytschko, T., Lu, Y.Y. and Gu, L. "Element-free Galerkin methods", *International Journal for Numerical Methods in Engineering*, **37**, pp. 229-256 (1994).
3. Wang, J. and Liu, G. "A point interpolation meshless method based on radial basis functions", *International Journal for Numerical Methods in Engineering*, **54**(11), pp. 1623-1648 (2002).
4. Liu, W.K., Jun, S. and Zhang, Y.F. "Reproducing kernel particle methods", *International Journal for Numerical Methods in Fluids*, **20**(8-9), pp. 1081-1106 (1995).
5. Koshizuka, S. and Oka, Y. "Moving-particle semi-

implicit method for fragmentation of incompressible fluid", *Nuclear Science and Engineering*, **123**(3), pp. 421-434 (1996).

6. Atluri, S. and Zhu, T. "A new meshless local Petrov-Galerkin (MLPG) approach in computational mechanics", *Computational Mechanics*, **22**(2), pp. 117-127 (1998).
7. Arzani, H. and Afshar, M. "Solving Poisson's equations by the discrete least square meshless method", *WIT Transactions on Modelling and Simulation*, **42**, pp. 23-31 (2006).
8. Shobeyri, G. and Afshar, M. "Simulating free surface problems using discrete least squares meshless method", *Computers & Fluids*, **39**(3), pp. 461-470 (2010).
9. Afshar, M. and Lashckarbolok, M. "Collocated discrete least-squares (CDLS) meshless method: Error estimate and adaptive refinement", *International Journal for Numerical Methods in Fluids*, **56**(10), pp. 1909-1928 (2008).
10. Firoozjaee, A.R. and Afshar, M.H. "Discrete least squares meshless method with sampling points for the solution of elliptic partial differential equations", *Engineering Analysis with Boundary Elements*, **33**(1), pp. 83-92 (2009).
11. Amani, J., Afshar, M.H. and Naisipour, M. "Mixed discrete least squares meshless method for planar elasticity problems using regular and irregular nodal distributions", *Engineering Analysis with Boundary Elements*, **36**(5), pp. 894-902 (2012).
12. Faraji, S., Afshar, M.H. and Amani, J. "Mixed discrete least square meshless method for solution of quadratic partial differential equations", *Scientia Iranica*, **21**(3), p. 492 (2014).
13. Afshar, M.H., Amani, J. and Naisipour, M. "A node enrichment adaptive refinement in discrete least squares meshless method for solution of elasticity problems", *Engineering Analysis with Boundary Elements*, **36**(3), pp. 385-393 (2012).
14. Afshar, M.H., Naisipour, M. and Amani, J. "Node moving adaptive refinement strategy for planar elasticity problems using discrete least squares meshless method", *Finite Elements in Analysis and Design*, **47**(12), pp. 1315-1325 (2011).
15. Nikravesh Kazeroni, S. and Afshar, M.H. "An adaptive node regeneration technique for the efficient solution of elasticity problems using MDLSM method", *Engineering Analysis with Boundary Elements*, **50**, pp. 198-211 (2015).
16. Liu, G.-R. and Gu, Y.-T., *An Introduction to Meshfree Methods and Their Programming*, Springer (2005).
17. Cao, Y., Yao, L. and Yin, Y. "New treatment of essential boundary conditions in EFG method by coupling with RPIM", *Acta Mechanica Solida Sinica*, **26**(3), pp. 302-316 (2013).
18. Wang, J. and Liu, G. "On the optimal shape parameters of radial basis functions used for 2-D meshless methods", *Computer Methods in Applied Mechanics and Engineering*, **191**(23), pp. 2611-2630 (2002).
19. Liu, G.-R., *Meshfree Methods: Moving Beyond the Finite Element Method*, Taylor & Francis (2009).
20. Timoshenko, S. and Goodier, J., *Theory of Elasticity*, 3rd Edition, New York: McGraw-Hill (1970).

Biographies

Siavash Nikravesh Kazeroni was graduated from Iran University of Science and Technology (IUST), Tehran, Iran, in late 2014, and received his master's degree in Civil Engineering-Hydraulic Structures major. His MS research focused on numerical analysis and mesh-free methods. This study was also presented as his master's seminar at IUST. Currently, he is pursuing his education and studying PhD in the University of New Mexico (UNM), NM, USA. His research fields consist of computational engineering, simulation, and structural analysis.

Mohammad Hadi Afshar obtained his BS degree in Civil Engineering from University of Tehran, Iran, and his MS and PhD degrees in University College of Swansea, Wales, UK. He is now an Associate Professor in the Civil Engineering Department at Iran University of Science and Technology (IUST), Tehran, Iran. His research interests include numerical modeling of solid and fluid mechanic problems and optimization methods.

Saeb Faraji received his MSc degree in Hydraulic Structures from Iran University of Science and Technology (IUST). Now, he is a PhD student in Amirkabir University of Technology working on mesh-free methods. His research interests include numerical simulation procedures focusing on mesh-free and finite element methods and their applications in elasticity and fluid problems.